ACSNANO

www.acsnano.org

ARTICLE

Analyzing Dirac Cone and Phonon Dispersion in Highly Oriented Nanocrystalline Graphene

Chang Tai Nai,[†,‡] Hai Xu,[†] Sherman J. R. Tan,[†,‡] and Kian Ping Loh*[,†]

[†]Department of Chemistry and Centre for Advanced 2D Materials (CA2DM), National University of Singapore, 3 Science Drive 3, Singapore 117543, Singapore

[‡]NUS Graduate School for Integrative Sciences and Engineering, National University of Singapore, Centre for Life Sciences, #05-01, 28 Medical Drive, Singapore 117456, Singapore

Supporting Information

ABSTRACT: **Chemical vapor deposition (CVD) is one of the most promising growth techniques to scale up the production of monolayer graphene. At present, there are intense efforts to control the orientation of graphene grains during CVD, motivated by the fact that there is a higher probability for oriented grains to achieve seamless merging, forming a large single crystal. However, it is still challenging to produce single-crystal graphene with no grain boundaries over macroscopic length scales, especially when the nucleation density of graphene nuclei is high. Nonetheless, nanocrystalline graphene with highly oriented grains may exhibit single-crystal-like properties. Herein, we investigate the spectroscopic signatures of graphene film containing highly oriented, nanosized grains (20−150 nm) using angle-resolved photoemission spectroscopy (ARPES) and high-resolution electron energy loss spectroscopy (HREELS). The robustness of the Dirac cone, as well as dispersion of its phonons, as a function of graphene's grain size and before and after film coalescence, was investigated. In view of the sensitivity of atomically thin graphene to atmospheric adsorbates and intercalants, ARPES and HREELS were also used to monitor the changes in spectroscopic signatures of the graphene film following exposure to the ambient atmosphere.**

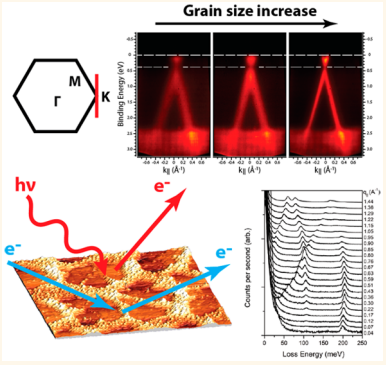

KEYWORDS: *chemical vapor deposition, graphene, Dirac cone, scanning tunneling microscopy, angle-resolved photoemission spectroscopy, high-resolution electron energy loss spectroscopy, phonon dispersion, ambient exposure, oxygen intercalation*

The two-dimensional monatomic thickness of graphene means that grain boundaries have a significant impact on electron transport properties.[1] The promise of chemical vapor deposition (CVD) graphene lies in its amenability to large-scale production,[2] but since it is a bottom-up growth process involving Ostwald's ripening of carbon nuclei, it invariably produces a polycrystalline film.[3−5] While there have been efforts to increase the grain size of CVD graphene, grain boundaries are still unavoidable across macroscopic length scales.[3,6,7] One question is whether the structure of the grain boundaries in graphene can be engineered to influence its electronic and mechanical properties.[5] Density Functional Theory (DFT) first-principles quantum transport calculations showed that the type of grain boundary formed, as well as the transport property of the graphene film, is dependent on the relative orientation of the grains adjacent to each other.[8] Symmetric and low-angle grain boundaries possess sufficient overlap of the Dirac cones of both grains, becoming essentially transparent to electrons, while grain boundaries characterized by large angle differences will create a transport gap due to the mismatch. Hence, control over the alignment of the grains will allow the grain boundaries and the electrical transport properties of the film to be manipulated.

Grain orientation of polycrystalline graphene has been studied using dark field transmission electron microscopy (TEM) and electron diffraction, which allows direct observation of the differently oriented grains stitched together into a quilt-like continuous film.[4,9] While TEM enables an intuitive visualization of the grain orientations, spectroscopic methods provide insights on other properties, such as the electronic structure. Surface science techniques that are sensitive to crystal orientation are potentially useful for this purpose. Micro- and nano-angle-resolved photoemission spectroscopy (ARPES) has been applied on polycrystalline graphene to characterize graphene−substrate electronic interaction[10] and the differences in doping and the Dirac point gap between different grain orientations.[11] A comparison between multigrain micro-ARPES and single-grain nano-ARPES has also been used to

Received: December 5, 2015
Accepted: December 29, 2015
Published: December 29, 2015

DOI: 10.1021/acsnano.5b07662
ACS Nano 2016, 10, 1681−1689

demonstrate the single-crystalline quality of a polycrystalline graphene film with micrometer-sized grains.[12]

Here, we performed ARPES using a laboratory-based monochromatic He II source with a spot size of 0.5 mm to study highly oriented nanocrystalline graphene prepared by plasma-assisted CVD on a (111)-textured Cu film (alloyed with 10% Ni) epitaxially grown on sapphire substrates. The highly oriented growth is enabled by the lattice matching between Cu and c-plane sapphire, which leads to the formation of highly oriented (111) Cu facets. In addition, angle-resolved high-resolution electron energy loss spectroscopy (HREELS) was performed to analyze the phonon dispersion.

Since graphene is an open surface, its electronic properties are readily modified by adsorbates or intercalants.[13−16] Adsorption of water and oxygen from the atmosphere has been demonstrated to result in p-type doping, masking the n-doping induced by substrate or grain boundaries. This was attributed to a competing electrochemical process that removes electrons from graphene.[17,18] To understand the evolution of the doping process starting from the as-grown film to after exposure to adsorbates such as oxygen and water, we applied surface-sensitive techniques such as ARPES and HREELS to monitor the changes in spectroscopic signatures.

RESULTS AND DISCUSSION

Figure 1a show the atomic force microscopy (AFM) topography images of a typical nanocrystalline graphene sample after 50 s of growth in an inductively coupled plasma CVD (ICP-CVD) system, where a dense distribution of nanoscale graphene islands can be seen; the angular edges and smooth surface of graphene are seen in the magnified AFM image in Figure 1b. The exposed Cu substrate was likely to be oxidized upon exposure to air, resulting in the roughening of the surface surrounding the graphene grains. Similar observations were made by scanning tunneling microscopy (STM) (Figure 1c). It can be noted that at this stage of growth some of the graphene grains have started to merge into larger domains. The average grain size can be estimated to be around 100 nm by measuring the lateral width of the grain just before coalescence using AFM. By tuning the growth conditions, nanocrystalline graphene films with grain sizes of 25, 50, and 100 nm, respectively, can be prepared. The graphene grain grows by lateral epitaxy, and a continuous film can be formed in 150 s using the plasma-assisted CVD process here.

The ordered hexagonal lattice of the graphene film was revealed by atomic resolution STM, demonstrating the high quality of the film. These atomically resolved STM images also allow the determination of the lattice orientation of the graphene grains. Figure 1d shows a typical region where a graphene film crosses a step on the underlying Cu substrate. By studying the orientation of the hexagonal lattice, it is clear that the graphene lattice retains the same orientation across the step, indicating continuous epitaxial growth that extends over the Cu substrate surface. High-magnification STM images sampled at several regions that are millimeters apart on the continuous graphene film, using the same scanning parameters and direction, show that the hexagonal lattices are mostly aligned. This is further corroborated by the fast Fourier transform of the images (Figure S1, Supporting Information), which show that different regions across large length scale on the surface have hexagonal lattices that are aligned in the same direction. A minority population is rotated ∼30° away from the majority direction, giving rise to disordered grain boundaries

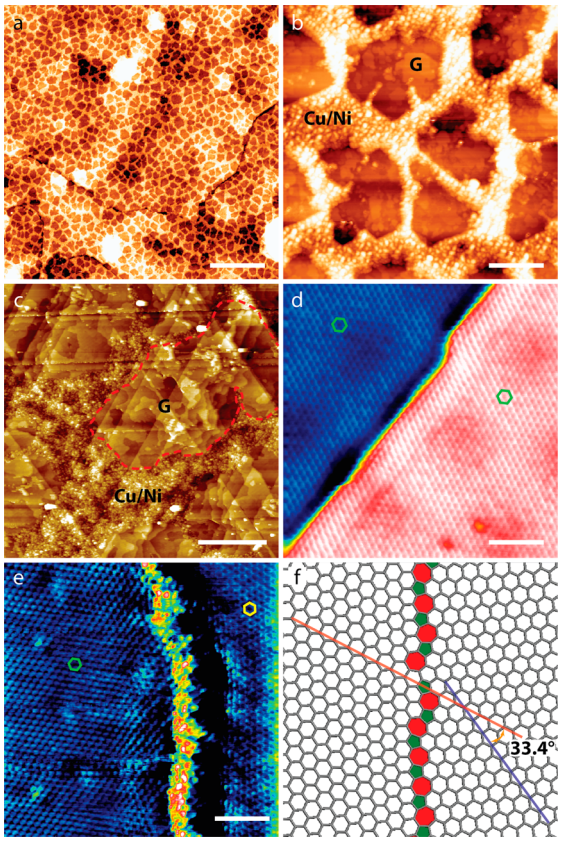

Figure 1. (a) AFM topography images of graphene grains before complete coalescence. (b) Magnified AFM topography image of the graphene nanograins in (a). (c) STM image of the graphene nanograins before coalescing into a film (V_s = −0.6 V, I_t = 800 pA). Red dotted line outlines one of the graphene domains. (d) Magnified STM image of the graphene film across a step. (e) Magnified STM image of a grain boundary between two graphene grains that are rotated ∼33.4° with respect to each other. Hexagons in (d) and (e) demonstrate lattice orientation in the graphene grains. (f) Schematic of a possible structure of the grain boundary in (e). Scale bars are (a) 2 μm, (b) 200 nm, (c) 50 nm, and (d, e) 2 nm, respectively.

that can be observed in STM, such as that in Figure 1e, which is likely to comprise several pentagon−heptagon pairs, as shown in the schematic in Figure 1f. However, it should be noted that these misaligned grains occupy less than 5% of the area sampled in our STM study. The crystal lattice of the graphene nanograins has also been confirmed using micro-low-energy electron diffraction, where a 6-fold symmetric diffraction pattern characteristic of the graphene honeycomb lattice can be seen. Overlapping the main diffraction pattern is another set of diffraction spots that is rotated 30 degrees away, which agrees with the STM analysis of the nanocrystalline graphene film.

With longer growth time, the nanocrystalline grains merged into a continuous film. Figure 2 shows the ARPES of a continuous graphene film with 100 nm grains at different sections of the Brillouin zone of graphene, as illustrated by the schematic in Figure 2a. At the Γ point, faint parabolic σ bands of graphene can be seen, together with the bright d bands from the copper substrate (Figure S2, Supporting Information). Near the Fermi energy (Figure 2b), a small parabolic band that extends to 0.25 eV can be observed, which corresponds to the Cu surface state. The observed band agrees with that reported

DOI: 10.1021/acsnano.5b07662
ACS Nano 2016, 10, 1681−1689

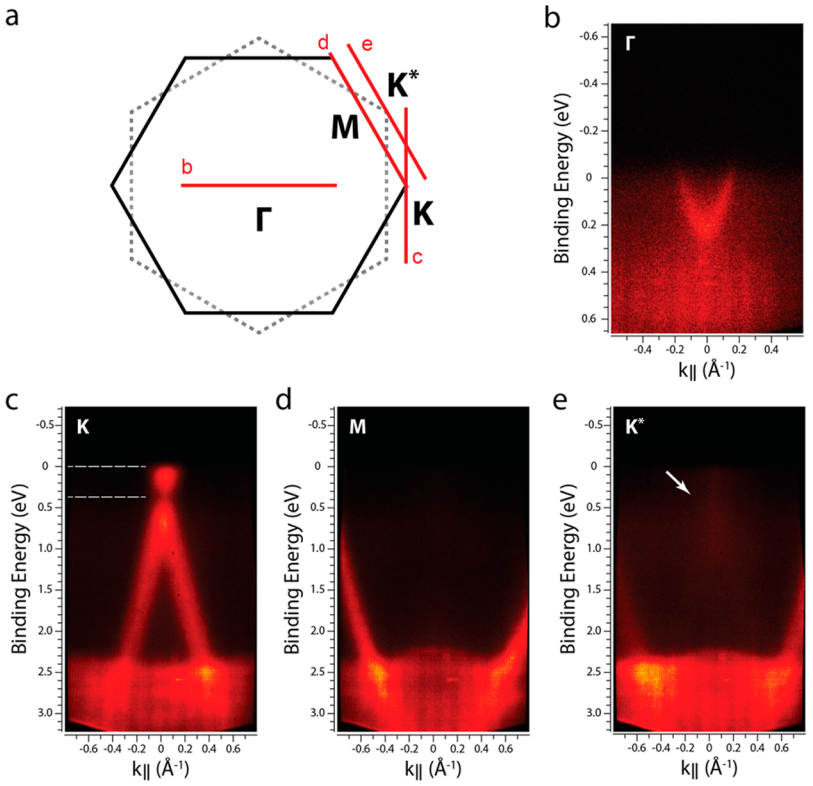

Figure 2. (a) Schematic illustrating the positions in the two-dimensional Brillouin zone for each photoelectron map (b−e). Dotted hexagon represents the Brillouin zone for a 30° rotationally displaced grain. ARPES mapping of continuous graphene sample at the (b) Cu surface state near the Fermi level at the Γ point, (c) K point, and (d) M point and (e) position off the K−M−K′ plane, denoted here as K*.

for graphene on Cu(111),[19] attesting to the high crystalline order of our Cu substrate.

At the K point (Figure 2c), the π bands of graphene can be observed very clearly, dispersing linearly near the Fermi energy and intersecting at the Dirac point at approximately 0.4 eV below the Fermi level. This is consistent with the n-doping of graphene on a copper surface.[11,20,21] The sharp Dirac point feature at the K point is observed only at 60° intervals when the sample is rotated azimuthally. The M point of the Brillouin zone can be probed along the K−M−K′ axis by rotating the azimuthal angle by 30° from the K point and reducing the polar angle to match the lower momentum, revealing a sharp parabolic π band valley as expected (Figure 2d).

However, by retaining the same polar angle as that at the K point while using the M point azimuthal angle, the region of the Brillouin zone being probed will then correspond to the region slightly off the K−M−K′ axis, as illustrated in the schematic in Figure 2a, which corresponds to the K point of a 30° rotated Brillouin zone (labeled as K*). Figure 2e shows the ARPES at this point, in which the parabolic π bands are more diffused, and a very faint Dirac cone can be observed in the middle (indicated with a white arrow). This faint Dirac cone is caused by a minority population of grains that are oriented approximately 30° away from the majority.

The analysis spot size under the angle dispersion mode used for ARPES is around 0.5 mm, which would average the signal contributions from at least 2.5×10^7 grains. Graphene film with randomly oriented grains will result in a ring of Dirac cones around the Γ point, due to the multitude of grain orientations within the scan spot.[11] It is interesting to note that we can observe rather sharp π bands for such a nanocrystalline sample, which suggest a high degree of orientation among the grains. The highly uniform grain orientation was supported by the STM observations, where the majority of the grains are observed to be oriented in the same direction, with a small minority oriented about 30° away.

The growth conditions can be tuned to produce different nucleation conditions, leading to nanocrystalline graphene films with different grain sizes. ARPES on these graphene samples with average grain sizes ranging from 50 to 150 nm demonstrates the changes in crystallinity caused by the different grain sizes. Figure 3a shows the K point of these samples, where it can be easily observed that the sample with smaller average grain size has much more diffused π bands, whereas the bands become sharper for larger grain size. Similarly, at the K* region, 30° from the K point (Figure 3b), faint Dirac cones (indicated with white arrows) can be observed for the 50 and 100 nm samples, indicating misalignment of grains, but practically no signal can be observed for the 150 nm sample. Since the grain sizes of these samples are many orders of magnitude smaller than the ARPES analysis spot size, the ARPES signals are averaged over many grains; thus the presence of a sharp Dirac cone around the K point indicates a high degree of grain uniformity.

In addition, the position of the Dirac point below the Fermi level remains relatively constant (white dotted lines in Figure 3a), despite the differences in the sharpness of the π bands. This indicates that the doping is primarily contributed by charge transfer interactions with the metallic substrate.

The ARPES of a discontinuous film with discrete grains that are ∼100 nm in size (30 s of growth time), as shown in Figure 4, also exhibits clear Dirac cones at 60° intervals around the Brillouin zone and faint ones rotationally offset by 30°, similar to the continuous film sample. This attests to the highly

DOI: 10.1021/acsnano.5b07662
ACS Nano 2016, 10, 1681−1689

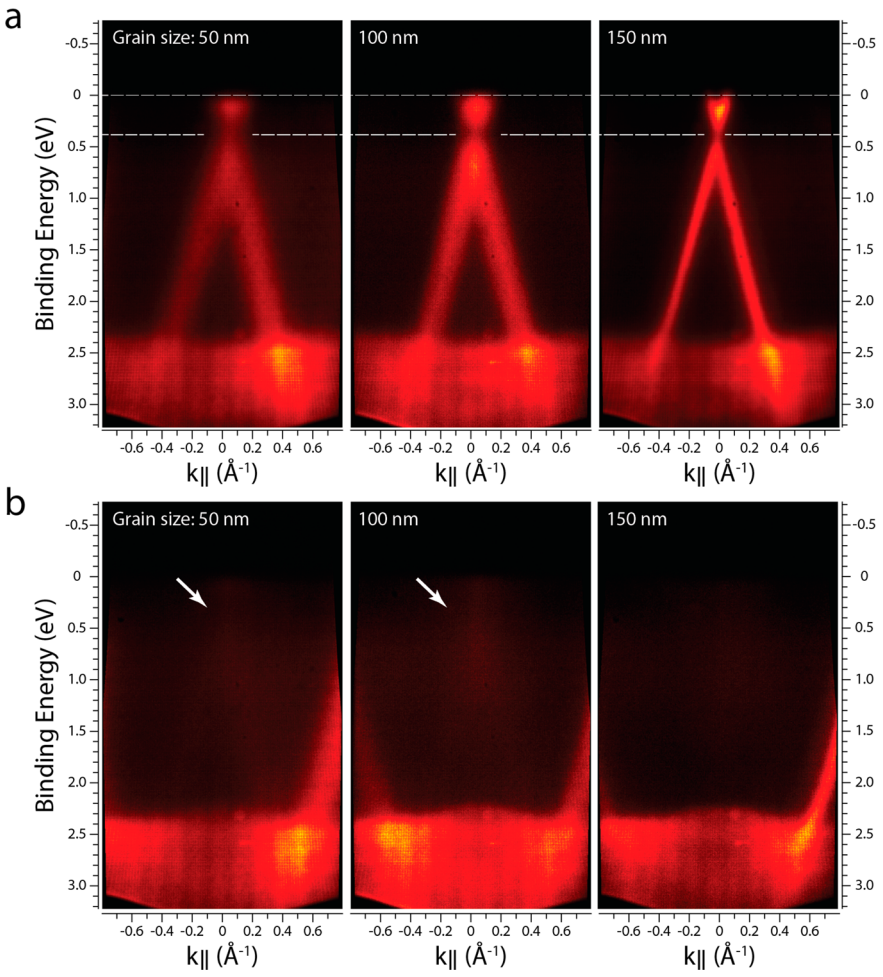

Figure 3. ARPES mapping of continuous graphene film with average grain sizes of 50, 100, and 150 nm at the (a) K point and the (b) K* point, respectively. White lines and arrows are guides for the eye to indicate the faint Dirac cones.

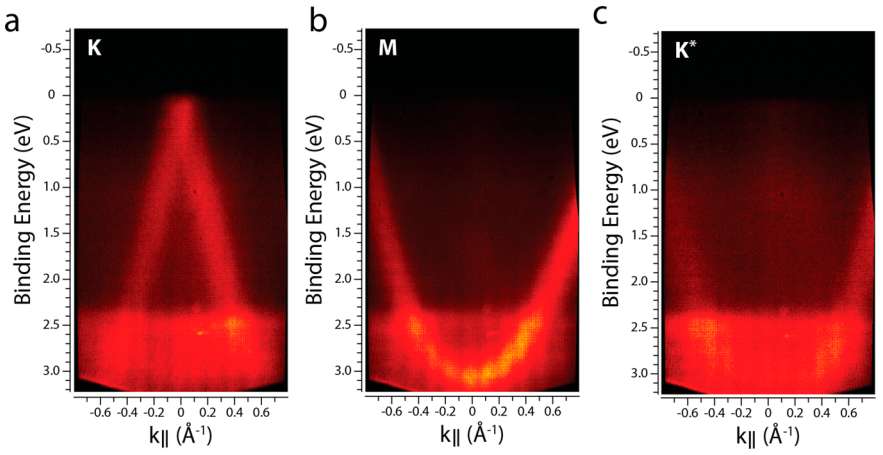

Figure 4. ARPES mapping of a discontinuous graphene islands sample at the growth time of 30 s, at the (a) K point, (b) M point, and (c) K* point. Refer to the schematic in Figure 2a for details on the position of each photoelectron map.

uniform orientation of the individual graphene grains on the sample even before they coalesce into a continuous film.

The ARPES of the graphene islands sample shows an interesting phenomenon. Figure 4a shows the ARPES at the K point of the discontinuous film, and it can be easily observed that, unlike that of a continuous film, the Dirac point is now at the Fermi level. The π band is more diffused, indicating an increase in orientation misalignment. It is evident from the scans at the K and M points that the entire π band has shifted upward toward the Fermi energy, while the Cu d bands show no shift. Hence, it can be deduced that there is little or no doping of the graphene islands, unlike that in the continuous film. A possible explanation for this phenomenon is that the intercalation of oxygen species beneath the individual grains occurs through the open edges during air exposure, leading to an irreversible oxidation of the Cu/Ni surface. This could also

DOI: 10.1021/acsnano.5b07662
ACS Nano 2016, 10, 1681−1689

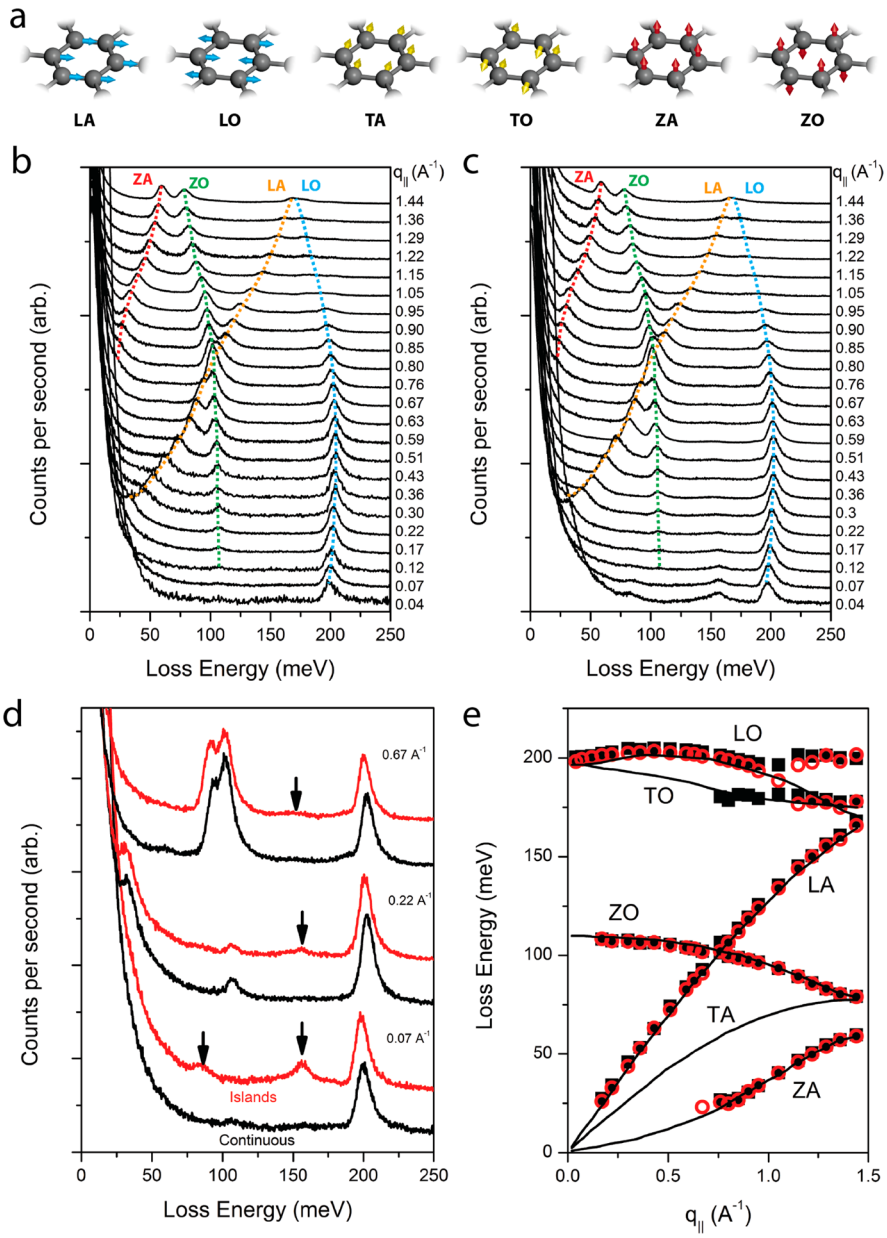

Figure 5. (a) Schematic of the six phonon modes of graphene with their classification based on the Γ−M direction. Angle-resolved HREELS of (b) a continuous graphene film at 150 s of growth and (c) discontinuous graphene islands at 30 s of growth, recorded in the Γ−M direction. The growth condition is such that the average grain size will be 100 nm when completely covered. Colored dotted lines are guides for the eye to follow the dispersion of the four main phonon peaks that can be observed, namely ZA (red), ZO (green), LA (orange), and LO (blue). (d) HREEL spectra of the continuous film and graphene islands at selected momentum for comparison. Arrows indicate points of difference. (e) Phonon dispersion obtained from the angle-resolved HREELS for the continuous film (solid squares) and the graphene islands (empty circles). The lines are theoretical phonon dispersion curves from Yanagisawa *et al.*[22]

explain the inability to observe a Cu surface state in the sample (Figure S3, Supporting Information). It has been reported that graphene grown on oxidized Cu(111) surfaces demonstrates a weaker doping effect than pure Cu(111),[20] and the X-ray photoelectron spectroscopy (XPS) of the discontinuous film samples also shows a higher oxygen content and some oxidation of Ni (Figure S4, Supporting Information). A continuous graphene film has fewer exposed edges and defects, making it harder for oxygen species to penetrate and oxidize the underlying metallic substrate. Hence, continuous films undergo stronger charge-transfer interaction with the substrate, leading to n-doping. Further investigation on the interaction of oxygen species with continuous graphene films will be discussed later.

HREELS probes vibrational and phonon modes of a surface through the scattering of incident electrons and is useful in observing phonon dispersion in momentum space due to the transfer of momentum during impact scattering. Graphene has two atoms in each unit cell, and multiplying that by the three axes of movement results in a total of six possible phonon modes, as illustrated in Figure 5a. These six modes can be categorized based on their direction as in-plane longitudinal (LO, LA), in-plane transverse (TO, TA), and out-of-plane (ZO, ZA) phonons, with each group consisting of both optical and acoustic variations based on whether the atoms move in or out of phase. Figure 5b,c show the HREEL spectra obtained at different scattering angles, along the Γ−M direction of the

DOI: 10.1021/acsnano.5b07662
ACS Nano 2016, 10, 1681−1689

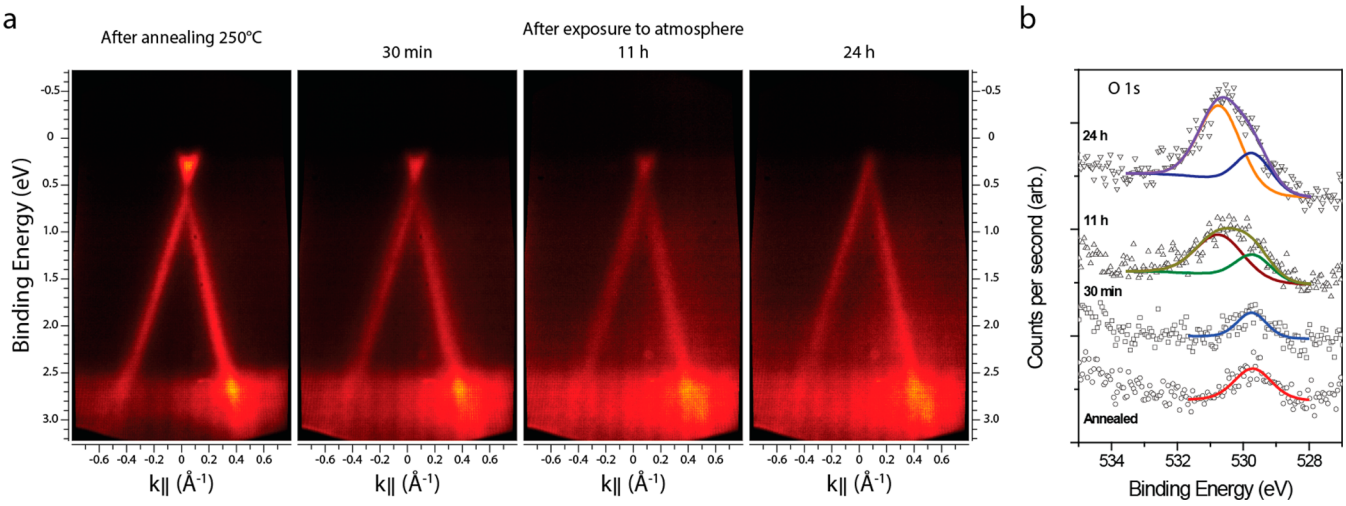

Figure 6. (a) ARPES mapping of the K point of a continuous graphene film before and after different durations of exposure to the atmosphere. (b) XPS O 1s peak of the graphene film before and after different ambient exposure for different times.

graphene samples. As graphene is a semimetallic homonuclear crystal, it lacks strong dipole fields and has conduction electrons that can cause shielding.[22] Therefore, the specular spectrum of graphene shows no detectable phonon peaks. In contrast, the off-specular loss spectra of graphene reveal a number of phonon peaks.

The angle-resolved HREEL spectra of a completely coalesced film with an average grain size of 100 nm and a discontinuous film with nearly coalesced grains of similar size show very similar phonon dispersion curves. Figure 5d shows a direct comparison between their loss spectra at a few selected $q_{||}$ values and demonstrates that both samples show the same phonon peaks with similar peak widths, indicating the high quality of the graphene grains even before they merge to form a continuous film. However, small differences can still be observed between the two samples. The graphene islands sample shows peaks at 84 and 152 meV at low $q_{||}$, but both peaks decrease in intensity with increasing values of $q_{||}$ and are absent in the continuous graphene film sample. The nondispersive property of these peaks suggests that it is not related to the phonons, and possible assignments for these peaks are γ(C−H), aromatic out-of-plane bending, and δ(C−H), in-plane bending, respectively.[23] Similar bending modes can be observed on aromatic molecules, such as benzene, deposited on metal surfaces.[23−25] The fact that these peaks are present only in the islands sample suggests that it could be due to hydrogen-terminated edges of the graphene grains, since the population of such edges is much lower in continuous graphene film.

Figure 5e shows the phonon dispersion of the two samples plotted against the theoretical dispersion reported by Yanagisawa *et al.*[22] The dispersion plot demonstrates that the phonon dispersions obtained for both samples are very similar and match the theoretical dispersion very well, indicating the good crystallinity of the graphene. It can be noted that the TA phonon is not observed in our sample, and components that may correspond to the TO phonon energy are only observed at a few $q_{||}$ values. This is due to the selection rule for HREELS whereby modes that are of odd parity under a reflection in the scattering plane are forbidden.[26] Under this selection rule, the TA and TO phonons are forbidden in the Γ−M direction, while the LO, TA, and ZO phonons are forbidden in the Γ−K direction. Other directions that do not pass through these high-symmetry points will exhibit no forbidden modes. As a result, polycrystalline samples that have randomly oriented grains will invariably exhibit the TA mode, as all directions will be contributing to the spectrum.[27−29] Hence, the absence of the TA phonon in the HREEL spectrum is indicative of the highly ordered orientation of the graphene film. The observation of weak components assignable to the TO modes at some $q_{||}$ values, even though the dispersion was measured in the Γ−M direction, could be due to the presence of some 30°-misaligned grains, on which the scattering plane will be along the Γ−K direction, where the TO phonon is not forbidden. Thus, it can be concluded here that the angle-resolved HREELS observations agree with that of the ARPES and STM.

To investigate the effects of ambient exposure, the continuous graphene films were removed from the ultrahigh-vacuum chamber and exposed to the atmosphere (Figure 6). After exposing to the atmosphere for a short period of time (30 min), the ARPES bands at the K point became more diffused, but the position of the Dirac point remained similar. However, increased atmospheric exposure time led to a gradual shift of the Dirac point toward the Fermi level, while the π bands became further diffused. Eventually, after 24 h of exposure, the Dirac point shifted to the Fermi level, demonstrating that exposure to ambient atmosphere resulted in a gradual loss of the n-doping in the clean sample.

Figure 6b shows the evolution of the O 1s peak in the XPS as the graphene film is being exposed to the atmosphere. Initially, after annealing the graphene film, trace amounts of oxygen still remain in the form of CuO (529.7 eV).[30] This is due to the slight oxidation of the copper surface. In agreement with the ARPES observations, short-term exposure to the atmosphere did not result in any significant changes in the O 1s spectrum. However, increasing the exposure duration led to the appearance of a new component at 530.7 eV, which became stronger with longer exposure time. The position of this peak matches the O 1s peak observed on Cu surfaces after dissociative adsorption of O_2[31] and is also similar to that observed for oxygen intercalation of graphene on Ru(0001).[32] In addition, no significant changes are observed in the C 1s and Cu 2p spectra (Figure S5, Supporting Information), implying that the increased oxygen content is not a result of the oxidation of the graphene or the substrate.

DOI: 10.1021/acsnano.5b07662
ACS Nano 2016, 10, 1681−1689

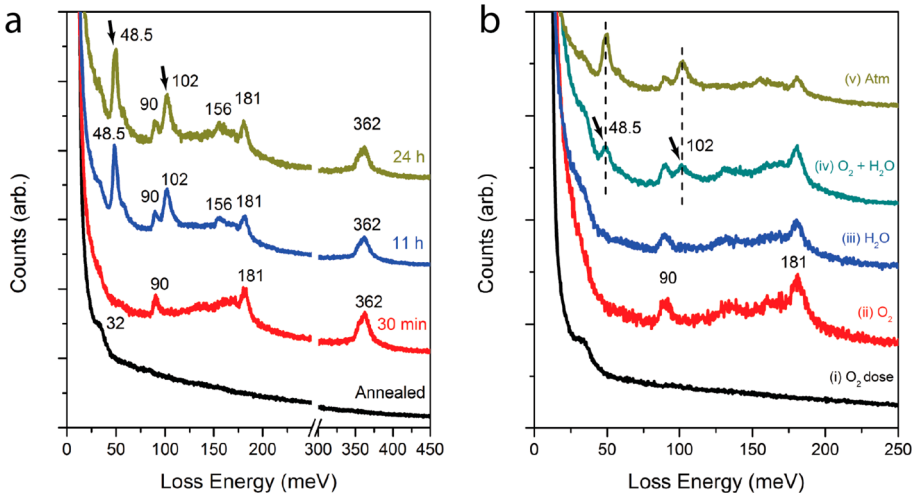

Figure 7. (a) HREEL spectra of a continuous graphene film before and after exposure to the atmosphere for different durations. Arrows indicate peaks that can be related to peroxo species on the Cu(111) surface. (b) HREEL spectra of a continuous graphene film after exposure to (i) 1.5 × 10^5 L O_2 with annealing at 160 °C, (ii) 1.5 bar (absolute pressure) O_2 for 60 h, (iii) 3 kPa H_2O for 20 h, and (iv) 1.5 bar (absolute pressure) O_2 and 3 kPa H_2O for 17 h. The HREEL spectrum of the film subjected to 24 h atmospheric exposure (v) is plotted for comparison.

HREELS was used to further elucidate the effect of atmospheric exposure on the graphene film. Figure 7a shows the specular HREEL spectra of the film before and after exposure to ambient air for different durations. As mentioned earlier, pristine graphene does not show phonon peaks in the specular HREELS; only a single peak at 32 meV can be observed, possibly due to surface phonon of the Cu substrate.[33] Exposure of the film to ambient air immediately leads to carbon contamination on the surface, manifesting in a number of energy loss peaks. The peak at 362 meV may be assigned to the ν(C−H) stretching mode, while the peaks at 156 and 181 meV are due to the $\delta(CH_2)$ bending modes, and the peak at 90 meV is assigned to the $\rho(CH_3)$ rocking mode.[34]

Prolonged exposure to ambient atmosphere (>11 h) led to the appearance of two strong peaks at 48.5 and 102 meV (indicated with arrows), which were not reported for the graphene/Pt(111) system. The appearance of these peaks coincides with the change in doping and increase in oxygen content observed in the ARPES and XPS, respectively. These peaks match the reported vibrational energies of ν(Cu−O) and ν(O−O) of peroxo species adsorbed on Cu(111), respectively.[35] Since the Cu substrate is completely covered by the graphene film, oxygen molecules have to penetrate through the grain boundaries of graphene in order to intercalate between graphene and the substrate. This limits the diffusion rate of the oxygen and explains why prolonged exposure duration is required for these changes to be observed.

The intercalation of oxygen explains the loss of n-doping in the graphene film.[19] Oxygen has an electron-withdrawing effect on the graphene film, leading to a counteracting p-doping effect on the graphene.[17,36] In addition, the intercalation of oxygen between graphene and the substrate effectively weakens the interaction between them, causing the graphene to become quasi-free-standing.[32] The overall effect is the gradual reduction of the n-doping of the graphene until it eventually becomes neutral.

To investigate the mechanism of the oxygen intercalation, a continuous graphene film was exposed in a controlled manner to oxygen and water followed by surface analysis with HREELS. Figure 7b shows the HREEL spectra obtained after different types of surface treatments. The peroxo-related peaks at 48.5 and 102 eV, which were observed when the sample was exposed to the atmosphere (Figure 7b(v)), could not be reproduced by exposing the sample in a vacuum to 1.5 × 10^5 L (Langmuir) of oxygen (Figure 7b(i)) and with the sample heated to 160 °C. These peaks also did not appear when the sample was exposed to either atmospheric pressures of O_2 or water alone (Figure 7b(ii),(iii)), which is reflective of the excellent ability of graphene to passivate the metal substrate against oxidation. Simultaneous dosing of O_2 and water was needed before the strong HREELS peaks due to the peroxo species appearing (Figure 7b(iv)). This observation suggests that the oxygen intercalation of Cu is most effective through an electrochemical process involving both O_2 and H_2O.

CONCLUSIONS

The crystalline quality of graphene grown on a (111)-textured Cu/sapphire substrate, when evolving from isolated grains to coalesced films, was monitored using surface spectroscopic techniques. The robustness of the Dirac cones in ARPES as well as the phonon dispersion profile in HREELS indicates the signatures of highly oriented grains in the film. Faint Dirac cones observed off the M point indicate that a small population of grains is rotated at ∼30° from the majority. These observations correlate well with the STM and angle-resolved HREELS observations. ARPES was also used to determine the robustness of the Dirac electronic spectra as a function of grain size. At the K point, well-defined conical Dirac dispersion can be seen for the graphene films with ∼50, ∼100, and ∼150 nm grain sizes. The bands in the Dirac cone are sharpest for films with ∼150 nm grains and become diffuse for films with smaller grain sizes. In addition, exposure to the ambient atmosphere reverses the n-doping of graphene due to oxygen intercalation between the film and the substrate. Exposure to both oxygen and water vapor allows oxygen intercalation to occur rapidly at the graphene−copper interface.

METHODS

Preparation of Graphene. Graphene islands or a continuous graphene film was grown on a Cu (alloyed with 10% Ni)-coated sapphire substrate in a cluster system equipped with sputtering and ICP-CVD. To obtain a highly textured (111)-Cu film, c-sapphire

DOI: 10.1021/acsnano.5b07662
ACS Nano 2016, 10, 1681−1689

substrates were sputtered with Cu and Ni in a composition of 10:1 to form an alloyed film. This was then treated with H_2 plasma at a gas flow rate of 100 sccm and a plasma power of 200 W for 5 min, with the substrate heated to 750−800 °C at 50 mTorr. To grow graphene, a mixture of H_2 and CH_4 (H_2:CH_4 = 10:1) was introduced into the chamber and the 200 W power plasma was ignited for more than 1 min, with the total pressure maintained at 50 mTorr. The growth time can be adjusted between 10 and 300 s to produce islands or a continuous film.

AFM. AFM measurements were performed with an XE-100 AFM (Park Systems) under ambient conditions in noncontact mode.

STM. The experiments were performed in an Omicron UHV system equipped with a low-temperature STM. The graphene samples were degassed at 120 °C overnight in a preparation chamber. STM was subsequently performed in the constant-current mode at liquid nitrogen temperature (77.8 K).

XPS and ARPES. Photoemission studies were performed in a UHV chamber with a base pressure of 3×10^{-10} mbar, equipped with a PHOIBOS 150 hemispherical energy analyzer (SPECS, GmbH) equipped with a 3D delay line detector (3D-DLD, SPECS GmbH), capable of both two-dimensional mapping and accumulative counting. The samples were degassed up to 250 °C for 1 h in a preparation chamber with a base pressure of 3×10^{-10} mbar to remove surface contaminants and then allowed to cool, before performing the measurements.

XPS was performed using the Mg Kα emission from the XR-50 X-ray source (SPECS GmbH), with a pass energy of 30 V on the analyzer. ARPES was performed using the He II emission from a differentially pumped UVS300 UV source (SPECS GmbH) that is monochromatized through a toroidal mirror monochromator (SPECS GmbH), with the analyzer capturing photoelectrons within a ±15° arc around the analyzer axis and performing a 2D mapping of the dispersion using the 3D-DLD.

HREELS. HREELS was performed using a Delta 0.5 spectrometer (SPECS, GmbH), in a UHV chamber with a base pressure of 2×10^{-10} Torr. For angle-resolved measurements, an incident electron energy of 20 eV is used, with an incident angle of 80° to the sample normal. The loss spectrum of the sample was collected at various scattered angles by rotating the analyzer and electron multipilier (Galileo 4830 U channeltron) between 75.3° and 20.9°. The phonon peaks were fitted using an exponential decay background and Lorentz peaks to determine their position.

Ambient Exposure. Graphene film samples were first degassed up to 250 °C for 1 h in a preparation chamber with a base pressure of 3×10^{-10} mbar to remove atmospheric contaminants and allowed to cool to room temperature before measurements.

After analyzing the annealed sample, it was removed from the UHV chamber and covered with a Petri dish to protect it from dust as it is exposed to the ambient environment. The sample was left in the ambient environment for 30 min, 11 h, and 24 h of total exposure time, respectively, before being replaced into the UHV chamber, and the various measurements were performed without further sample annealing or degassing.

Oxygen and Water Exposure. Clean graphene film was annealed as described above before the ambient exposure experiment. Oxygen dosing in UHV was performed by backfilling the chamber using a leak valve at a pressure of up to 3×10^{-6} mbar for a total of 19 h while the sample was heated to 160 °C. For atmospheric level exposures, the sample is placed in the load lock chamber. For oxygen exposure, purified oxygen gas was leaked into the load lock chamber through a ball valve with an absolute pressure of 1.5 bar. For water exposure, a sealed vial of water was connected to the load lock chamber *via* another ball valve and purified by freeze−evacuation cycles to remove dissolved gases. For simultaneous exposure of oxygen and water, both ball valves were opened at the same time.

ASSOCIATED CONTENT

Supporting Information

The Supporting Information is available free of charge on the ACS Publications website at DOI: 10.1021/acsnano.5b07662.

STM study of the highly oriented nanocrystalline graphene film at different regions, ARPES of the continuous film and islands at the Γ point, and XPS of the graphene sample at different growth times and different ambient exposure durations (PDF)

AUTHOR INFORMATION

Corresponding Author

*E-mail: chmlohkp@nus.edu.sg.

Notes

The authors declare no competing financial interest.

ACKNOWLEDGMENTS

We thank the support of National Research Foundation under its midsized Centre Program as well as the NRF-CRP grant "Towards commercialization of graphene technologies" R-143-000-546-281. We acknowledge Dr. Gao Libo for providing the ICP-CVD-grown samples for the ARPES and HREELS study while he was working in the Graphene Centre, NUS, under the supervision of K.P.L.

REFERENCES

(1) Peres, N. M. R.; Guinea, F.; Castro Neto, A. H. Electronic Properties of Disordered Two-Dimensional Carbon. *Phys. Rev. B: Condens. Matter Mater. Phys.* **2006**, *73*.10.1103/PhysRevB.73.125411

(2) Bae, S.; Kim, H.; Lee, Y.; Xu, X.; Park, J. S.; Zheng, Y.; Balakrishnan, J.; Lei, T.; Ri Kim, H.; Song, Y. I.; Kim, Y. J.; Kim, K. S.; Özyilmaz, B.; Ahn, J. H.; Hong, B. H.; Iijima, S. Roll-to-Roll Production of 30-Inch Graphene Films for Transparent Electrodes. *Nat. Nanotechnol.* **2010**, *5*, 574−578.

(3) Yu, Q.; Jauregui, L. A.; Wu, W.; Colby, R.; Tian, J.; Su, Z.; Cao, H.; Liu, Z.; Pandey, D.; Wei, D.; Chung, T. F.; Peng, P.; Guisinger, N. P.; Stach, E. A.; Bao, J.; Pei, S. S.; Chen, Y. P. Control and Characterization of Individual Grains and Grain Boundaries in Graphene Grown by Chemical Vapour Deposition. *Nat. Mater.* **2011**, *10*, 443−449.

(4) Huang, P. Y.; Ruiz-Vargas, C. S.; Van Der Zande, A. M.; Whitney, W. S.; Levendorf, M. P.; Kevek, J. W.; Garg, S.; Alden, J. S.; Hustedt, C. J.; Zhu, Y.; Park, J.; McEuen, P. L.; Muller, D. A. Grains and Grain Boundaries in Single-Layer Graphene Atomic Patchwork Quilts. *Nature* **2011**, *469*, 389−392.

(5) Tsen, A. W.; Brown, L.; Levendorf, M. P.; Ghahari, F.; Huang, P. Y.; Havener, R. W.; Ruiz-Vargas, C. S.; Muller, D. A.; Kim, P.; Park, J. Tailoring Electrical Transport Across Grain Boundaries in Polycrystalline Graphene. *Science* **2012**, *336*, 1143−1146.

(6) Gao, L.; Ren, W.; Xu, H.; Jin, L.; Wang, Z.; Ma, T.; Ma, L. P.; Zhang, Z.; Fu, Q.; Peng, L. M.; Bao, X.; Cheng, H. M. Repeated Growth and Bubbling Transfer of Graphene with Millimetre-Size Single-Crystal Grains Using Platinum. *Nat. Commun.* **2012**, *3*, 699.

(7) Lee, J. H.; Lee, E. K.; Joo, W. J.; Jang, Y.; Kim, B. S.; Lim, J. Y.; Choi, S. H.; Ahn, S. J.; Ahn, J. R.; Park, M. H.; Yang, C. W.; Choi, B. L.; Hwang, S. W.; Whang, D. Wafer-Scale Growth of Single-Crystal Monolayer Graphene on Reusable Hydrogen-Terminated Germanium. *Science* **2014**, *344*, 286−289.

(8) Yazyev, O. V.; Louie, S. G. Electronic Transport in Polycrystalline Graphene. *Nat. Mater.* **2010**, *9*, 806−809.

(9) Kim, K.; Lee, Z.; Regan, W.; Kisielowski, C.; Crommie, M. F.; Zettl, A. Grain Boundary Mapping in Polycrystalline Graphene. *ACS Nano* **2011**, *5*, 2142−2146.

(10) Wilson, N. R.; Marsden, A. J.; Saghir, M.; Bromley, C. J.; Schaub, R.; Costantini, G.; White, T. W.; Partridge, C.; Barinov, A.;

DOI: 10.1021/acsnano.5b07662
ACS Nano 2016, 10, 1681−1689

Dudin, P.; Sanchez, A. M.; Mudd, J. J.; Walker, M.; Bell, G. R. Weak Mismatch Epitaxy and Structural Feedback in Graphene Growth on Copper Foil. *Nano Res.* **2013**, *6*, 99−112.
(11) Avila, J.; Razado, I.; Lorcy, S.; Fleurier, R.; Pichonat, E.; Vignaud, D.; Wallart, X.; Asensio, M. C. Exploring Electronic Structure of One-Atom Thick Polycrystalline Graphene Films: A Nano Angle Resolved Photoemission Study. *Sci. Rep.* **2013**, *3*, 2439.
(12) Brown, L.; Lochocki, E. B.; Avila, J.; Kim, C.-J.; Ogawa, Y.; Havener, R. W.; Kim, D.-K.; Monkman, E. J.; Shai, D. E.; Wei, H. I.; Levendorf, M. P.; Asensio, M.; Shen, K. M.; Park, J. Polycrystalline Graphene with Single Crystalline Electronic Structure. *Nano Lett.* **2014**, *14*, 5706−5711.
(13) Liu, H.; Liu, Y.; Zhu, D. Chemical Doping of Graphene. *J. Mater. Chem.* **2011**, *21*, 3335−3345.
(14) Chen, W.; Chen, S.; Dong, C. Q.; Xing, Y. G.; Wee, A. T. S. Surface Transfer p-Type Doping of Epitaxial Graphene. *J. Am. Chem. Soc.* **2007**, *129*, 10418−10422.
(15) Politano, A.; Marino, A. R.; Chiarello, G. Effects of a Humid Environment on the Sheet Plasmon Resonance in Epitaxial Graphene. *Phys. Rev. B: Condens. Matter Mater. Phys.* **2012**, *86*.10.1103/PhysRevB.86.085420
(16) Yang, Y.; Brenner, K.; Murali, R. The Influence of Atmosphere on Electrical Transport in Graphene. *Carbon* **2012**, *50*, 1727−1733.
(17) Ryu, S.; Liu, L.; Berciaud, S.; Yu, Y. J.; Liu, H.; Kim, P.; Flynn, G. W.; Brus, L. E. Atmospheric Oxygen Binding and Hole Doping in Deformed Graphene on a SiO_2 Substrate. *Nano Lett.* **2010**, *10*, 4944−4951.
(18) Pinto, H.; Jones, R.; Goss, J. P.; Briddon, P. R. Mechanisms of Doping Graphene. *Phys. Status Solidi A* **2010**, *207*, 2131−2136.
(19) Walter, A. L.; Nie, S.; Bostwick, A.; Kim, K. S.; Moreschini, L.; Chang, Y. J.; Innocenti, D.; Horn, K.; McCarty, K. F.; Rotenberg, E., Electronic Structure of Graphene on Single-Crystal Copper Substrates. *Phys. Rev. B: Condens. Matter Mater. Phys.* **2011**, *84*.10.1103/PhysRevB.84.195443
(20) Gottardi, S.; Müller, K.; Bignardi, L.; Moreno-López, J. C.; Pham, T. A.; Ivashenko, O.; Yablonskikh, M.; Barinov, A.; Björk, J.; Rudolf, P.; Stöhr, M. Comparing Graphene Growth on Cu(111) *versus* Oxidized Cu(111). *Nano Lett.* **2015**, *15*, 917−922.
(21) Marsden, A. J.; Asensio, M. C.; Avila, J.; Dudin, P.; Barinov, A.; Moras, P.; Sheverdyaeva, P. M.; White, T. W.; Maskery, I.; Costantini, G.; Wilson, N. R.; Bell, G. R. Is Graphene on Copper Doped? *Phys. Status Solidi RRL* **2013**, *7*, 643−646.
(22) Yanagisawa, H.; Tanaka, T.; Ishida, Y.; Matsue, M.; Rokuta, E.; Otani, S.; Oshima, C. Analysis of Phonons in Graphene Sheets by Means of HREELS Measurement and *ab initio* Calculation. *Surf. Interface Anal.* **2005**, *37*, 133−136.
(23) Shen, W.; Nyberg, G. L.; Liesegang, J. An Electron Spectroscopic Study of the Adsorption of Benzenethiol and 1,2-Benzenedithiol on the Cu(110) Surface. *Surf. Sci.* **1993**, *298*, 143−160.
(24) Lutterloh, C.; Biener, J.; Pöhlmann, K.; Schenk, A.; Küppers, J. Modification of the Benzene-Metal Interaction by C and H Monolayers at Pt(111) Surfaces. *Surf. Sci.* **1996**, *352*−*354*, 133−137.
(25) Allegretti, F.; De Renzi, V.; Biagi, R.; del Pennino, U.; Contini, G.; Di Castro, V.; Mariani, C.; Betti, M. G.; Fontanesi, C. HREELS Study of the Adsorption Mechanism and Orientational Order of 2-Mercaptobenzoxazole on Cu(100). *Surf. Sci.* **2003**, *539*, 63−71.
(26) De Juan, F.; Politano, A.; Chiarello, G.; Fertig, H. A. Symmetries and Selection Rules in the Measurement of the Phonon Spectrum of Graphene and Related Materials. *Carbon* **2015**, *85*, 225−232.
(27) Aizawa, T.; Hwang, Y.; Hayami, W.; Souda, R.; Otani, S.; Ishizawa, Y. Phonon Dispersion of Monolayer Graphite on Pt(111) and NbC Surfaces: Bond Softening and Interface Structures. *Surf. Sci.* **1992**, *260*, 311−318.
(28) Politano, A.; Marino, A. R.; Chiarello, G., Phonon Dispersion of Quasi-Freestanding Graphene on Pt(111). *J. Phys.: Condens. Matter* **2012**, *24*.10402510.1088/0953-8984/24/10/104025
(29) Oshima, C.; Aizawa, T.; Souda, R.; Ishizawa, Y.; Sumiyoshi, Y. Surface Phonon Dispersion Curves of Graphite (0001) over the Entire Energy Region. *Solid State Commun.* **1988**, *65*, 1601−1604.
(30) Mariot, J. M.; Barnole, V.; Hague, C. F.; Vetter, G.; Queyroux, F. Local Electronic Structure of Cu_2O, CuO and $YBa_2Cu_3O_{7-\delta}$. *Z. Phys. B: Condens. Matter* **1989**, *75*, 1−9.
(31) Rajumon, M. K.; Prabhakaran, K.; Rao, C. N. R. Adsorption of Oxygen on (100), (110) and (111) Surfaces of Ag, Cu and Ni: An Electron Spectroscopic Study. *Surf. Sci.* **1990**, *233*, L237−L242.
(32) Zhang, H.; Fu, Q.; Cui, Y.; Tan, D.; Bao, X. Growth Mechanism of Graphene on Ru(0001) and O_2 Adsorption on the Graphene/Ru(0001) Surface. *J. Phys. Chem. C* **2009**, *113*, 8296−8301.
(33) Menezes, W.; Knipp, P.; Tisdale, G.; Sibener, S. J. Surface Phonon Spectroscopy of Ni(111) Studied by Inelastic Electron Scattering. *Phys. Rev. B: Condens. Matter Mater. Phys.* **1990**, *41*, 5648−5651.
(34) Kato, H. S.; Noh, J.; Hara, M.; Kawai, M. An HREELS Study of Alkanethiol Self-Assembled Monolayers on Au(111). *J. Phys. Chem. B* **2002**, *106*, 9655−9658.
(35) Sueyoshi, T.; Sasaki, T.; Iwasawa, Y. Molecular and Atomic Adsorption States of Oxygen on Cu(111) at 100−300 K. *Surf. Sci.* **1996**, *365*, 310−318.
(36) Zhou, H.; Qiu, C.; Yu, F.; Yang, H.; Chen, M.; Hu, L.; Guo, Y.; Sun, L. Raman Scattering of Monolayer Graphene: The Temperature and Oxygen Doping Effects. *J. Phys. D: Appl. Phys.* **2011**, *44*.18540410.1088/0022-3727/44/18/185404

DOI: 10.1021/acsnano.5b07662
ACS Nano 2016, 10, 1681−1689